ARTICLE

Seaweed-Derived Hierarchically Porous Carbon for Highly Efficient Removal of Tetracycline

Wen-xiu Qin[a†], Na Sun[b†], Guo-zhong Wang[a], Hai-min Zhang[a], Yun-xia Zhang[a*]

a. Key Laboratory of Materials Physics, Centre for Environmental and Energy Nanomaterials, Anhui Key Laboratory of Nanomaterials and Nanotechnology, CAS Centre for Excellence in Nanoscience, Institute of Solid State Physics, Chinese Academy of Sciences, Hefei 230031, China
b. School of Chemical and Environmental Engineering, Anhui Polytechnic University, Wuhu 241000, China

(Dated: Received on September 2, 2020; Accepted on September 16, 2020)

Herein we present a facile approach for the preparation of a novel hierarchically porous carbon, in which seaweeds serve as carbon source and KOH as activator. The fabricated KOH-activated seaweed carbon (K-SC) displays strong affinity towards tetracycline (TC) with maximum uptake quantity of 853.3 mg/g, significantly higher than other TC adsorbents. The superior adsorption capacity ascribes to large specific surface area (2614 m^2/g) and hierarchically porous structure of K-SC, along with strong π-π interactions between TC and K-SC. In addition, the as-prepared K-SC exhibits fast adsorption kinetics, capable of removing 99% of TC in 30 min. Meanwhile, the exhausted K-SC can be regenerated for four cycling adsorption without an obvious degradation in capacities. More importantly, pH and ionic strengths barely affect the adsorption performance of K-SC, implying electrostatic interactions hardly play any role in TC adsorption process. Furthermore, the K-SC packed fixed-bed column (0.1 g of adsorbents) can continually treat 2780 mL solution spiked with 5.0 mg/g TC before reaching the breakthrough point. All in all, the fabricated K-SC equips with high adsorption capacity, fast adsorption rate, glorious anti-interference capability and good reusability, which make it hold great feasibilities for treating TC contamination in real applications.

Key words: Hierarchically porous carbon, Tetracycline, Adsorption mechanism, Fixed-bed column

I. INTRODUCTION

Over the past decades, various antibiotics have been universally used to handle bacterial infections and as husbandry growth promoters [1]. The widespread utilization and even abuse of antibiotics have posed adverse effects to human health and ecosystem [2]. As a typical broad-spectrum antibiotic, tetracycline (TC) is deemed as the most widely applied antibiotics. Similar to most other antibiotics [3], TC is barely taken in or absorbed by organisms, discharging about 25%−75% of the total TCs into environment through excretion [4]. As a consequence, TC is frequently measured in surface water, groundwater and soil, which promotes antibiotic-resistant bacterias rapid propagation, inevitably causing serious threats to public health and ecological balance [5]. Furthermore, the TC eliminating efficiency by traditional water treatment technologies is usually unsatisfactory. Thus, exploiting high-efficiency and practical techniques for removing TC from contaminative environments is of great need.

Recently, a variety of methods have been proposed for removing TC from water, including adsorption, membranes separation, chemical oxidation, biodegradation, photocatalytic or photoelectrocatalytic degradation *etc.* [6−8]. Due to the antibacterial nature of TC, biodegradation cannot achieve desirable results for the alleviating of TC. Although chemical oxidation and photocatalytic degradation have been regarded as the most promising technique for TC mineralization [9], the expensive reactants, complex operating process and potential secondary pollution prevent their practical application. Even worse, some intermediate degradation by-products of TC exhibit significantly higher toxicity than that of TC [8]. By contrast, adsorption is identified as technically and economically suitable techniques for TC removal, in view of its fast removal rate, high efficiency, simple operation and no production of harmful byproducts. So far, different types of adsorbent materials are fabricated and applied in TC elimination, such as, zeolite [10], goethite [11], clay minerals [12], car-

---

[†] These authors contributed equally to this work.
[*] Author to whom correspondence should be addressed. E-mail: yxzhang@issp.ac.cn

DOI:10.1063/1674-0068/cjcp2009154

bon nanotubes [13], graphene oxide [14, 15], and active carbon [16]. Of all the above adsorbents, carbon-based adsorbents have attracted more attention for TC removal, in view of their high specific area, hierarchically porous structures and low weight [17]. Furthermore, a large number of π electrons reside in carbon materials, which can bind strongly with TC via π-π interactions and consequently demonstrate optimal TC immobilization efficiencies, thereby rendering carbon-based materials to be fascinating adsorbents for TC remediation [18].

The activated carbon (AC) derived from petroleum sources has been proven to exhibit high adsorption capacity towards TC [19]. However, its production cost is relatively high in regard of the applied raw materials and activating agents. Thus, there is growing interests in developing cost effective, easy scale-up adsorbents for TC removal. Taking into account the greatest renewable carbon-rich resource in nature, biomass materials and wastes are extensively utilized for the fabrication of carbon-based adsorbents due to their low-cost, renewability, easy availability and environmentally friendly advantage [20]. For example, agriculture wastes [21, 22], nutshells [23], resins [24], *etc.*, have been applied as adsorbents to remove TC from waters. However, these biomass-derived carbon adsorbents are still face with several inherent limitations, such as small specific surface area, poor porosity, limited accessibility of raw materials, as well as low adsorption capacities, which hinder their practical applications. As a consequence, developing low-cost and effective absorption materials with super-high specific surface area, hierarchically porous structures along with abundant functional groups for TC elimination is still an urgent task.

Marine alga seaweed species, as the abundant and renewable resources in vast sea area, have been widely utilized in pharmaceutical, cosmetics, fertilizers and food industries due to their intrinsic chemical composition [25]. Annually, the production of seaweeds exceeds 19 million tons [26], suggesting their easy accessibility. In addition, seaweeds possess considerably porous cell walls, various functional groups and inorganic ingredients [27]. The inorganic ingredients often serve as porogen for producing porous carbon materials. These features make seaweeds fantastic precursors for producing porous carbon materials enriched with hierarchical porosity and surface functionality. Recently, seaweed-derived biochar has been utilized in agriculture and horticulture in view of their plentiful nutrient contents [28]. Besides, seaweed biomass has been used for preparing porous carbon material applied in the new energy field, including supercapacitor and fuel cells [29, 30]. However, there is very little attention about the conversion of seaweeds into hierarchically porous carbon activated by KOH and their application in TC removal.

Based on these considerations mentioned above, we present a facile method to prepare a novel adsorbent K-SC for highly efficient TC removal, in which easily available natural seaweed and KOH serve as the precursor and the activating agent, respectively. Applying seaweeds as carbon source for constructing porous carbon can not merely lower manufacturing price, but also easily achieve mass production. The utilization of KOH is in view of its low activating temperature, short activating duration, and well developed pore structure [31]. Batch experiments including uptake kinetics and isotherms are conducted for evaluating the adsorption performance of the fabricated K-SC towards TC. Meanwhile, influences of solution pH and ionic strengths on TC removal are also investigated. Furthermore, the underlying mechanism for TC removal by K-SC is elucidated based on Fourier transform infrared spectroscopy (FT-IR) and X-ray photoelectron spectroscopy (XPS) analyses before and after TC adsorption. Since the post-separation process of adsorbents is time-consuming and high cost, the continuous fixed bed adsorption will be a more promising approach for practical application [32]. In view of this, we construct a fixed bed adsorption device by combining an adsorption column, an automatic collector and a flow pump to test the adsorption potential of K-SC for TC in a continuous-flow process.

II. EXPERIMENTAL SYNTHESIS OF KOH-ACTIVATED SEAWEED CARBON

The collected seaweeds were fully cleaned by DI water and freeze dried. Subsequently, the pretreated seaweeds were annealed at N_2 atmosphere with 5 °C/min to 700 °C for 60 min to obtain the precursor-seaweed carbon (SC). Subsequently, SC was further dipped in 100 mL of 2 mol/L HCl under stirring for 12 h at ambient temperature without any sonication and then flushed with DI water, drying at 60 °C under vacuum. After that, SC was reserved in a vacuum dryer for further use. To further get KOH-activated seaweed carbon (K-SC), the activating agent KOH was mixed with SC with a ratio of KOH:SC=4:1 (g/g) and the mixtures were annealed at N_2 atmosphere to 800 °C for 120 min. Subsequently, the K-SC was completely rinsed by HCl (2 mol/L) and DI water to exclude the remaining activating agent and other inorganic species. In the end, the resulted K-SC was dried at 60 °C and collected for further application.

III. RESULTS AND DISCUSSION

A. Morphological and structural characterizations of SC and K-SC

The seaweed derived hierarchically porous carbon is synthesized by a facile two-step carbonization on the basis of our former research [29], as shown in Scheme 1. Briefly, SC is got from a simple pyrolysis treatment

DOI:10.1063/1674-0068/cjcp2009154

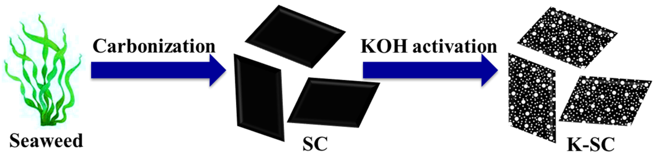

Scheme 1. Illustration of the construction of the seaweed-derived hierarchically porous carbon.

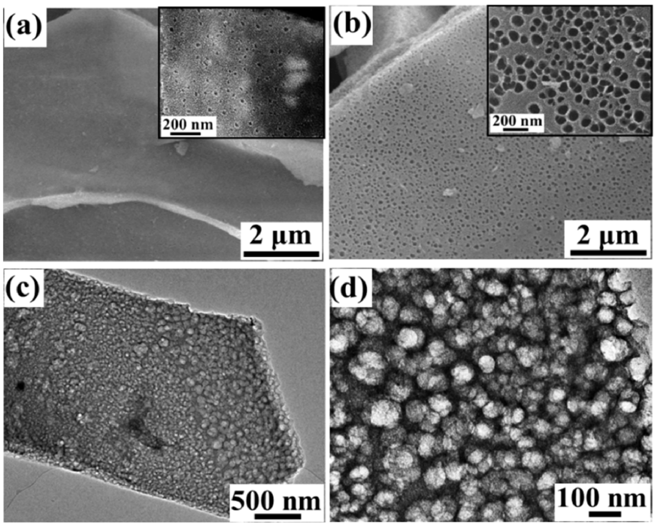

FIG. 1 SEM images of (a) SC and (b) K-SC. (c, d) The representative TEM characterizations for K-SC.

of seaweed in an inert atmosphere. To further obtain K-SC, the SC is mixed with the activator KOH, which is subsequently subjected to carbonization treatment under 800 °C for 120 min. The morphologies of SC and K-SC are observed by SEM and TEM. As displayed in FIG. 1(a), the pristine SC presents a sheet-like structure with a small amount of pore structure; while after activated by KOH, numerous holes with various sizes are uniformly and densely distributed on the K-SC surface (FIG. 1(b)). The magnified SEM image of K-SC (the insert in FIG. 1(b)) shows that numerous mesopores and macropores spread throughout the whole surface and inner of the sheet-like structure, suggesting the successful construction of hierarchical pores during the activating process. TEM characterization (FIG. 1(c, d)) further confirms the construction of hierarchical pores in K-SC, which will improve the accessibility of the active sites, consequently facilitating the elimination efficiency of TC.

To further identify the porosity of SC and K-SC, nitrogen adsorption-desorption isotherm analysis is conducted. As displayed in FIG. 2(a), SC and K-SC exhibit representative type IV behaviors with the presence of hysteresis, indicating micro- and mesopores coexisting in them. The specific Brunauer-Emmett-Teller (BET) surface area of SC is computed to be 329 $\mathrm{m^2/g}$, which is expanding to 2614 $\mathrm{m^2/g}$ for K-SC. It follows that the injection of KOH greatly enhances the surface area values of K-SC, which can be ascribed to the interaction between KOH and carbon at high temperatures [23]. Correspondingly, the dimension distribution of pores along with overall pore volumes also aggrandize after the activation of KOH, as reflected by two new peaks appearing at 1.8 and 2.4 nm (FIG. 2(b)). The total pore volumes of SC and K-SC are calculated by using the Barret-Joyner-Halenda (BJH) method to be 0.22 and 1.4 $\mathrm{cm^3/g}$, respectively. The above results demonstrate that the introduction of KOH enlarges the surface areas as well as dimension distribution of pores in K-SC, in accordance with the SEM observations.

Meanwhile, XRD is utilized to investigate the crystal structure of the as-prepared products. As illustrated in FIG. 2(c), both SC and K-SC have two wide diffraction peaks (002) located at 25° and (100) located at 43°, ascribed to reflections of graphitic structures [33], which suggests that graphitized carbon is successfully fabricated from seaweed through the pyrolysis reaction. Raman spectroscopy is further employed to analyze the molecular structure of SC and K-SC. As seen from FIG. 2(d), both SC and K-SC display two peaks at around 1350 and 1590 $\mathrm{cm^{-1}}$, which represent the D-band and G-band, respectively. As usual, D-band stands for the disorder and defects of graphitic carbon, while G-band corresponds to sp^2-hybridized carbon in well-ordered graphite [34]. The intensity ratios of two bands (*i.e.* $I_\mathrm{D}/I_\mathrm{G}$) for SC and K-SC are 1.02 and 1.05, respectively, suggesting more defects are formed after the activation of KOH. Evidently, higher intensity of D-band in K-SC illustrates the lower graphitization degree, which is resulted from intense reaction between carbon and KOH [35].

Since chemical bond properties play important roles in the elimination performance of the adsorbents, surface functional groups of SC and K-SC are characterized by FT-IR spectroscopy. FIG. S3 in supplementary materials illustrates the FT-IR spectra of SC and K-SC. The FT-IR spectra of SC and K-SC are similar, and the major absorption bands at 3436, 1629 and 1400 $\mathrm{cm^{-1}}$ are assigned to the stretching oscillation of hydroxyl, aromatic carbon-oxygen double bond, carbon-carbon double bond and phenolic C−O−H bending, respectively [36]. Besides, the band at 667 $\mathrm{cm^{-1}}$ is assigned to out-of-plane angular deformations of aromatic rings [37]. These results imply the existence of oxygen-bearing chemical bonds (-OH and -COOH bonds) in SC and K-SC, which will significantly enhance the hydrophilic properties of adsorbents and act as binding sites for TC.

The chemical structures of SC and K-SC are further confirmed by XPS technique. As demonstrated in the overall XPS spectrum in FIG. 3(a), C, N and O elements exist in the SC and K-SC. The calculated atomic percent of C, N and O in SC are 64.35%, 3.61% and 31.04%, respectively. After being activated by KOH, the atomic percent of N and O in K-SC decrease to

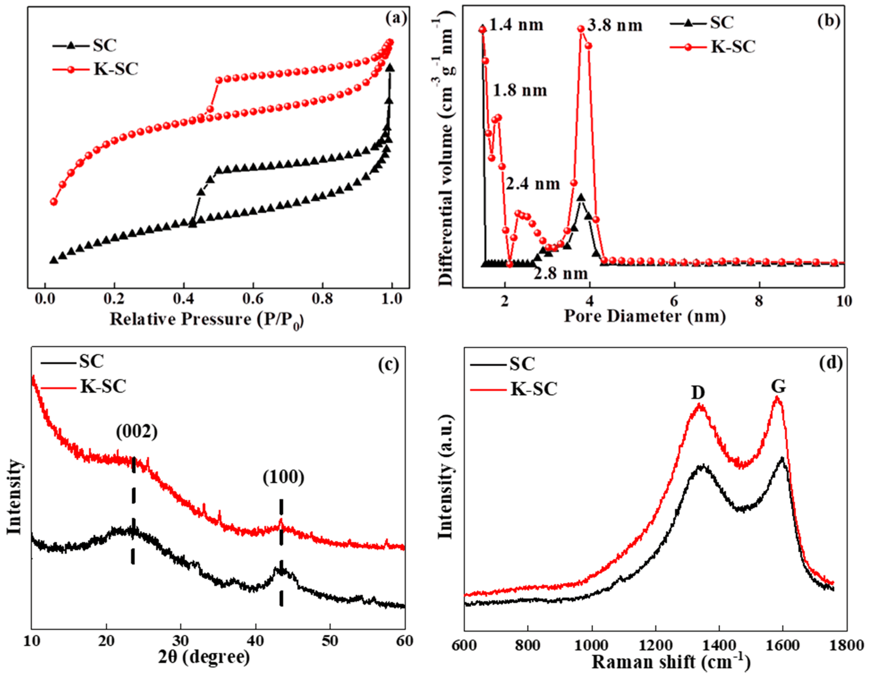

FIG. 2 (a) N_2 adsorption-desorption isotherms and (b) corresponding pore size distributions of SC and K-SC, (c) XRD characteristics, (d) Raman of SC and K-SC.

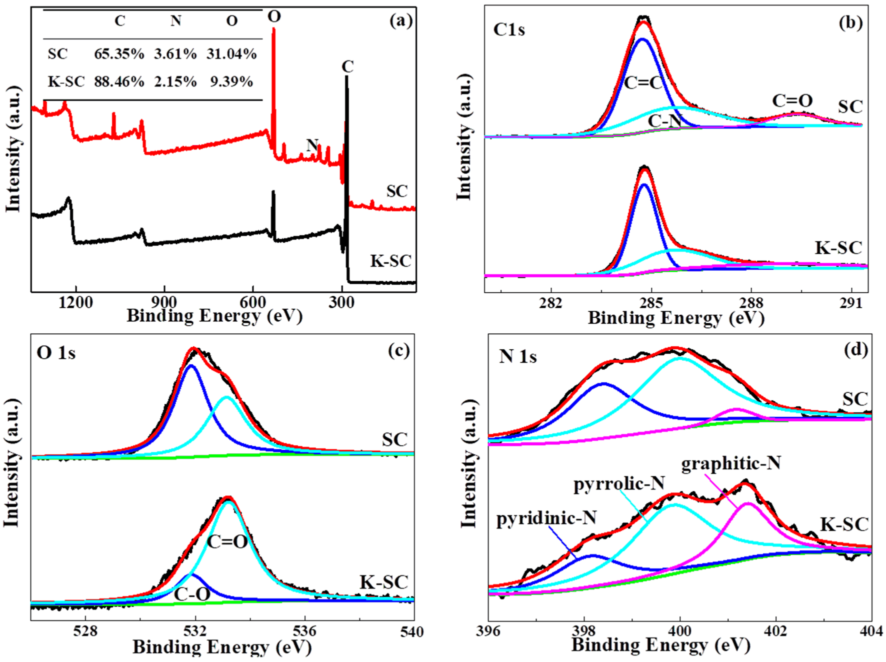

FIG. 3 XPS spectra of SC and K-SC: (a) survey spectrum, (b) C 1s, (c) O 1s, (d) N 1s.

2.15% and 9.39%, accompanied by the increase of C content (88.46%), which is attributed to that the non-carbon elements is prone to decompose in the presence of KOH [29]. After deconvolution in FIG. 3(b), C 1s is divided into three peaks at binding energy of 284.7 eV (indexed to C=C), 285.6 eV (indexed to CCN) and 289.2 eV (indexed to C=O), respectively. Due to the decrease of O content of K-SC, the intensity of C=O in K-SC is significantly lower than that in SC. The high resolution O 1s spectra of SC and K-SC (FIG. 3(c)) are divided into two peaks, which are assigned to C=O (531.7 eV) and C−O (533.2 eV), further confirming the existence of oxygen-bearing chemical bonds in the resulting carbon adsorbents, favorable for enhanc-

DOI:10.1063/1674-0068/cjcp2009154

TABLE I Kinetic parameters for TC adsorption on K-SC.

C_0/(mg/L)	Pseudo-first-order kinetic			Pseudo-second-order kinetic		
	q_e/(mg/g)	k_1/(min^{-1})	R^2	q_e/(mg/g)	k_2/(g·mg^{-1}·min^{-1})	R^2
10	3.1	4.03×10^{-2}	0.415	100.2	2.07×10^{-1}	0.999
30	8.8	4.15×10^{-2}	0.539	312.5	1.21×10^{-2}	0.999
50	15.9	3.74×10^{-2}	0.703	495.0	2.87×10^{-3}	0.999

TABLE II Langmuir and Freundlich isotherm parameters for TC adsorption onto SC and K-SC.

Adsorbents	Langmuir model			Freundlich model		
	$q_{\max}$/(mg/g)	$K_{\rm L}$/(L/mg)	R^2	$K_{\rm F}$/(mg/g)	$1/n$	R^2
SC	216.7	0.04	0.997	25.7	0.41	0.937
K-SC	853.3	0.42	0.743	440.9	0.15	0.928

ing the elimination capability of adsorbents. The N 1s spectrum can be deconvoluted into three peaks at 398.1, 400.1 and 401.1 eV, assigned to the binding energies of pyridinic-N, pyrrolic-N and graphitic-N, respectively (FIG. 3(d)). Previous studies have shown that pyridinic-N and graphitic-N possess excellent potentiality of electron transfer [29]. Evidently, the graphitic-N content (25.78%) of K-SC is much higher than that of SC (8.38%), implying its strong π-π interaction capacity, which are favorable for the adsorption of TC.

B. Adsorption kinetic studies of TC onto SC and K-SC

The adsorption performance of SC and K-SC towards TC at different contact time is determined and the results are illustrated in FIG. 4(a). Obviously, the elimination rate of TC by SC is relatively dilatory, and only 42.8% of TC is removed after 24 h. As for K-SC, nearly all of TC can be adsorbed within 30 min under the identical conditions, indicating that KOH activation greatly enhanced the elimination performance of K-SC. Furthermore, the adsorption performance of K-SC at different TC concentrations (10, 30, 50 mg/L) was studied. As shown in FIG. 4(b), regardless of initial concentrations, TC can be dramatically adsorbed by K-SC at the beginning 10 min, which can achieve equilibrium after 60 min. To elucidate the adsorption mechanism of TC on K-SC, the pseudo-first-order models (PFOM) (Eq.(1)) and pseudo-second-order models (PSOM) (Eq.(2)) are applied for simulating the experimental data [38].

$$\ln(q_{\rm e}-q_t) = \ln q_{\rm e} - k_1 t \tag{1}$$

$$\frac{t}{q_t} = \frac{1}{(k_2 {q_{\rm e}}^2)} + \frac{t}{q_{\rm e}} \tag{2}$$

where $q_{\rm e}$, q_t, k_1 and k_2 denote quantity of TC uptake by K-SC after reaching equilibration and time t (min), the rate constants of PFOM and PSOM (g·mg^{-1}·min^{-1}), respectively. All the dynamical parameters and coefficients (R^2) calculated from two models are revealed in Table I. It can be seen that the R^2 values calculated from Pseudo-second-order kinetic (PSOM) are much higher than that of Pseudo-first-order kinetic (PFOM), suggesting that PSOM is more appropriate for describing the kinetic process. The well-fitting of PSOM confirm that chemisorption is the speed-limiting step for TC adsorbed on K-SC, similar adsorption behaviors have been reported on other TC adsorbents [18]. Notably, k_2 decrease from 2.07×10^{-1} g·mg^{-1}·min^{-1} to 2.87×10^{-3} g·mg^{-1}·min^{-1} with TC concentrations increasing from 10 mg/L to 50 mg/L, which can be ascribed to much more furious scramble for surface active sites at higher concentration [39].

C. Adsorption isotherms of TC onto SC and K-SC

To further evaluate the adsorption capacity of SC and K-SC towards TC, adsorption isotherms are conducted at various primary TC contents (5.0−200 mg/L) at pH=7.0. As can be seen from FIG. 5, the elimination abilities of SC and K-SC towards TC increase with raising the TC concentrations. Note that the uptake capacity of TC by K-SC is significantly higher than that on SC, suggesting that KOH activation greatly enhance the elimination capability of adsorbents. Furthermore, Langmuir and Freundlich isotherm models are used to elucidate the interaction between adsorbent and TC. The fitted parameters for these two models are summarized in Table II. Obviously, the correlation coefficients (R^2) of the Langmuir and Freundlich isotherm models for SC are 0.997 and 0.937, respectively. Thus, the Langmuir model can preferably fit the adsorption isotherms than the Langmuir model, suggesting that the TC adsorption on SC is a monolayer adsorption. As for K-SC, the R^2 of Freundlich model (0.928) is larger than that of Langmuir model (0.743), suggesting that the TC adsorption on K-SC belongs to the heterogeneous surface adsorption. In addition, the separation factors ($R_{\rm L}$) (calculated from Eq.(S4) in supplementary materials) of Langmuir model for SC and K-SC

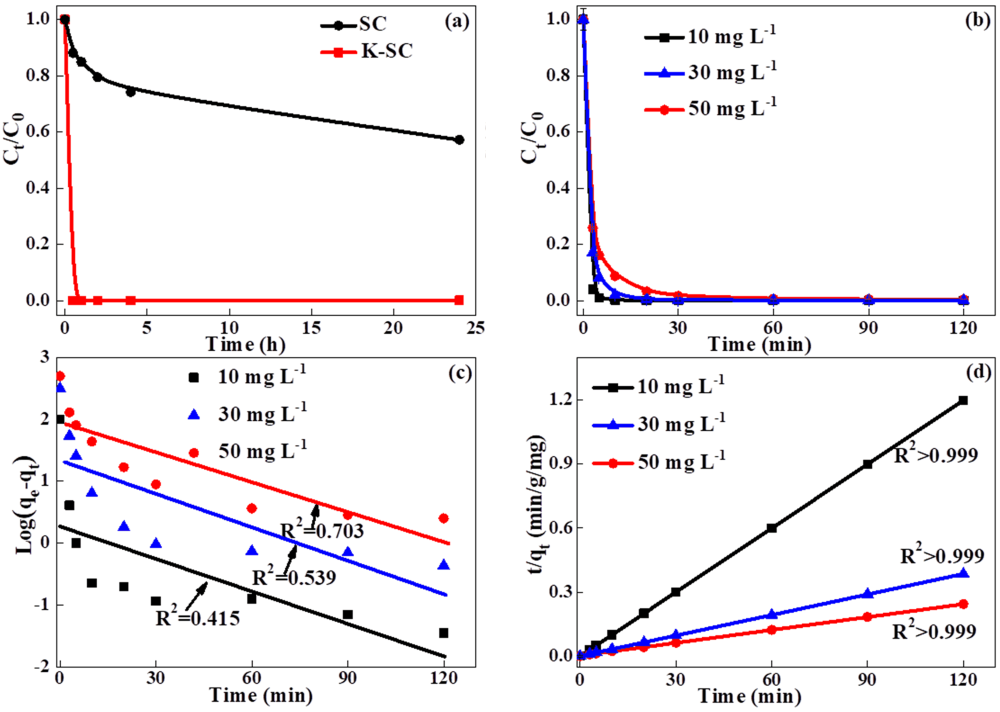

FIG. 4 (a) Adsorption kinetic studies of SC and K-SC, (b) effects of initial TC concentrations on K-SC performance, (c) pseudo-first order model fitting, (d) pseudo-second order model fitting. Experimental conditions: initial TC concentration=10−50 mg/L, adsorbents contents=0.1 g/L, equilibrium time=24 h, initial pH=7.0, temperature=25 °C.

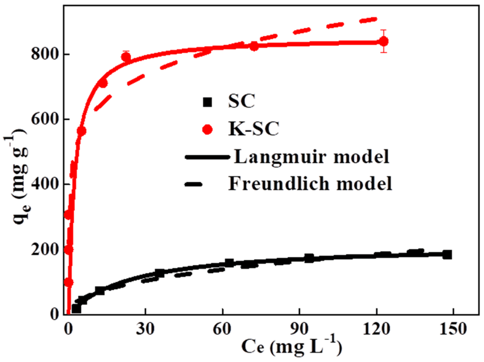

FIG. 5 Adsorption isotherms of SC and K-SC towards TC fitted to Langmuir model (the solid line) and Freundlich model (the dash line). Experimental conditions: initial TC concentration=5.0−180 mg/L, adsorbents contents=0.1 g/L, equilibrium time=24 h, initial pH=7.0, temperature=25 °C.

are all between 0 and 1, which illustrates the adsorption process for the as-prepared adsorbents is favorable. Likewise, the n values (connected with the adsorption capacity) calculated from Freundlich model are all in excess of 1.0 for both SC and K-SC, revealing that TC adsorbed by the adsorbents is a favorable process. In addition, the maximum TC adsorption capacities for SC and K-SC are calculated to be 216.6 and 853.3 mg/g, respectively. Importantly, the uptake capacity of K-SC is much higher than other biomass-derived TC adsorbents, as summarized in Table III, which may benefit from the large surface area and hierarchically porous structure of K-SC.

D. Impact of pH on TC elimination efficiency

The solution pH can significantly affect the existing speciation of TC and surface charges of adsorbents, accordingly influence the interactions between adsorbate and adsorbents as well as the adsorption capacities. Thus, the effects of pH on TC elimination efficiency are investigated. As displayed in FIG. 6(a), K-SC exhibits strong affinity towards TC at all pH conditions (pH=3.0−9.0). Under acid and neutral conditions, the elimination efficiency of TC is more than 99% within 30 min. With the solution pH rising to 9.0, TC elimination efficiency is slightly decreased to 97% (the inset in FIG. 6(a)), which might be related to the zero potential charge (pH_{ZPC}) of K-SC and the charged conditions of TC. As shown in FIG. S2 (supplementary materials), at pH>9.0, TC is negatively charged with the main existing form of TCH^- and $TC_2{}^-$ [4]. Additionally, the pHZPC of K-SC is estimated to be 5.2 according to the relationship between zeta potentials and pH (FIG. 6(b)). Considering the dominant TC species of TCH^- and $TC_2{}^-$ at pH>9.0, the negative surface charges of K-SC are not favorable for the adsorption of negatively charged TC. In view of the fact that the ad-

TABLE III The maximum adsorption capacities of various adsorbents towards TC

Adsorbents	Surface area/(m^2/g)	Adsorption capacity/(mg/g)	References
Alfalfa-derived biochar	31.1	372.3	[40]
Human hair carbon	1505	210.1	[41]
Apricot stone carbon	307.6	308.3	[42]
Tyre carbon	814	356	[17]
Clay composite	43.1	76.0	[12]
Alkali biochar	117.8	58.8	[43]
Sludge-based adsorbent	126.9	87.9	[44]
Agave and Tanin carbon	1068	239.4	[45]
magnetic porous carbon	349	30.0	[46]
K-SC	2614	853.3	This work

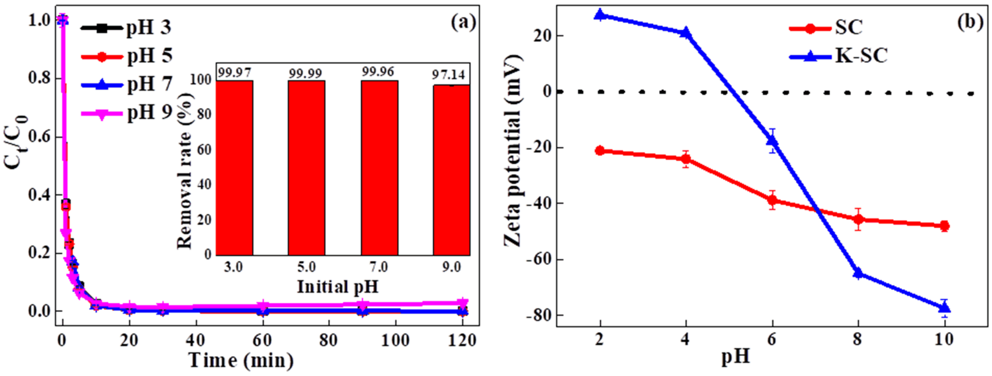

FIG. 6 (a) Impacts of pH on the TC elimination efficiency; (b) Zeta potential of SC and K-SC. Experimental conditions: original TC contents=30 mg/L, adsorbents contents=0.1 g/L, equilibration time=2.0 h, temperature=25 °C.

sorption amount of TC decreases very little due to the electrostatic repulsion, the strong adsorption of TC by K-SC is not governed by electrostatic adsorption. This is further confirmed by the high removal efficiency of TC at low pH conditions. At pH=3.0, TC is positively charged (existing as TCH_3^+), at the same time the surface charge of K-SC is positive, in which the adsorption of TC may be restrained through the principle of the same charge repulsion. The high adsorption efficiency of TC under acid conditions indicates that except for electrostatic interaction, the specific π-π interaction occurs between the TC and K-SC, in line with early TC elimination studies [18].

E. Influences of ionic strengths on TC elimination efficiency

The influences of ionic strengths on TC elimination efficiency by K-SC are studied by conducting a series of adsorption experiments at four different $NaNO_3$ concentrations (1.0, 10, 50, 100 mmol/L). As illustrated in FIG. 7(a), the adsorption efficiency of TC always remains at a high level with the $NaNO_3$ concentration increasing from 1.0 mmol/L to 100 mmol/L. Moreover, PSOM can perfectly fit the adsorption kinetics of TC and all the correlation coefficients are above 0.999. Besides, there is no significant difference in adsorption rate constants with the $NaNO_3$ concentration increasing from 1.0 mmol/L to 100 mmol/L (the inset in FIG. 7(a)). This phenomenon indicates that ionic strengths have little impacts on TC elimination efficiency, even in high concentrations, further confirming the specific π-π interactions play vital roles in the strong affinity of K-SC towards TC.

F. Reusability of K-SC on the elimination of TC

To evaluate the reusability of the adsorbents, the adsorption-desorption cycle experiments are conducted by exposing a certain amount of K-SC in TC solutions (30 mg/L). After the adsorption is finished, the used adsorbents are collected by vacuum filtration, desorbed by a mixture solution containing 2% (W/W) NaOH and 50% ethyl alcohol solutions (V/V) for 1 h, afterward adequately flushed with DI water to neutral pH and dried. Then, the regenerated adsorbents are redispersed in the fresh TC solution and the next cycle of adsorption is conducted. As displayed in FIG. 7(b), after the fifth run, the removal efficiency of TC is still more than 97%, indicating the excellent reusability of K-SC as adsorbents.

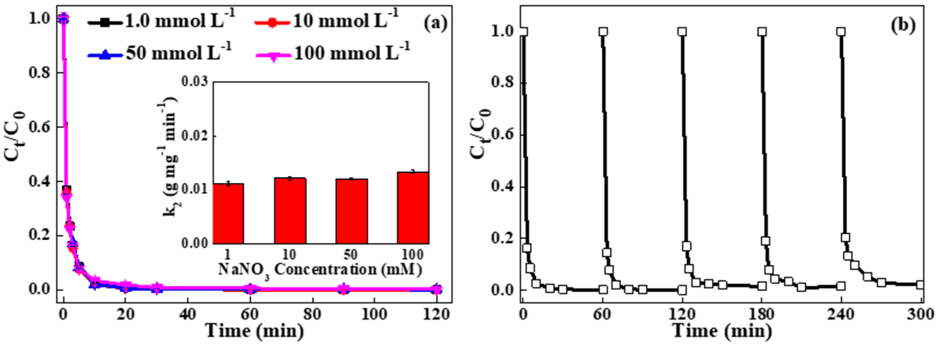

FIG. 7 (a) Influences of ionic strengths on TC elimination efficiency and the corresponding rate constants fitted by PSOM (the insert). (b) Recycling study of the adsorption performance of TC on the K-SC. Experimental conditions: original TC contents=30 mg/L, adsorbents contents=0.1 g/L, initial pH=7.0, temperature=25 °C.

G. TC elimination mechanisms

In order to better elucidate the TC elimination mechanisms by K-SC, FT-IR and XPS are employed for investigating the composition variations of K-SC before and after use. As shown in FIG. S4(a) in supplementary materials, some changes occur in the chemical bonds of K-SC after combining with TC, for instance, the bond of OCH stretching shifts from 3436 cm^{-1} to 3451 cm^{-1}, the peaks of C=O and C=C shift from 1629 cm^{-1} to 1641 cm^{-1}, suggesting that the functional groups of K-SC are of great importance for TC elimination through extensive hydrogen bonding or strong π-π interaction [47]. Simultaneously, the changes of vibration bands in the region from 1200 cm^{-1} to 1800 cm^{-1} further confirm the specific π-π interaction in the process of TC elimination [47]. The ketone groups in TC act as π-electron-acceptors in view of its glorious electron-withdrawing competence, consequently interacting forcefully with the abundant polarized π electrons in graphite surface of K-SC.

Besides FT-IR characterization, XPS technique is also applied to clarify the variations of K-SC binding energies before and after uptake TC. After adsorbing TC, the atomic percentages of N and O in K-SC increase from 2.15% to 2.48% and from 9.39% to 16.43% (FIG. S4(b) in supplementary materials), respectively, which are ascribed to the rich nitrogen and oxygen-bearing chemical bonds in the TC and give solid evidence to the strong interaction between K-SC and TC. FIG. S4(c) in supplementary materials shows the high resolution C 1s spectra of K-SC before and after binding TC. As displayed, the content of C=O groups in K-SC-TC increases dramatically after adsorbing TC due to the rich ketone groups of TC. It is noteworthy that O1s spectrum shifts from 533.1 eV to low binding energy of 532.28 eV (FIG. S4(d) in supplementary materials); at the same time intensities of both C=O and CCO peaks increase in view of high content of phenol and ketone groups in TC. For the pristine K-SC, N 1s spectrum is deconvoluted to three peaks at binding energy of 398.1 (pyridinic-N), 400.1 (pyrrolic-N) and 401.1 eV (graphitic-N), respectively. It is noteworthy that a novel N 1s peak assigned to -NH$_2$ emerges at 402.3 eV after adsorbing TC, implying the successful loading of TC on K-SC. Moreover, the pyridinic-N and graphitic-N contents of K-SC-TC decrease significantly from 20.99% to 0.1% and from 25.78% to 17.58%, respectively, which further confirm the strong electron transfer between the nitrogen-containing functional groups in K-SC and TC. On the basis of the above analyses, we can conclude that the plausible TC adsorption mechanism is the integrated effects of strong π-π interaction as well as forming hydrogen bonding, in which the strong π-π interactions assume primary responsibility for the elimination of TC.

H. Fixed bed experiment

The above batch experiments indicate that the as-prepared K-SC can be utilized for effective TC elimination in the real environmental water systems. However, the collection of the spent adsorbents is time consuming and high cost. By contrast, the continuously operated fixed bed is a very plausible way for *in-situ* TC elimination from the aqueous environment. Thus, we use K-SC to load the fixed-bed column for examining the TC elimination efficiency in different situations. As demonstrated in FIG. 8(a), the elimination process reaches saturation fast when SC is applied as adsorbents. As for K-SC, in light of the high elimination capacity along with fast adsorption rate, the breakthrough and exhaustion time remarkably increase, with the efficient purification volume of 2780 breakthrough volumes (BV) when the breakthrough point is set as the interception rate of 95%. The TC quantity uptake by K-SC at this breakthrough point of the packed column is calculated to be 139 mg/g, almost eight times as much as the previously reported breakthrough point of 18.53 mg/g (methanol-modified biochar as adsorbents) [48]. The influences of flow rate on TC elimination efficiency in the fixed bed column are also studied. As

DOI:10.1063/1674-0068/cjcp2009154

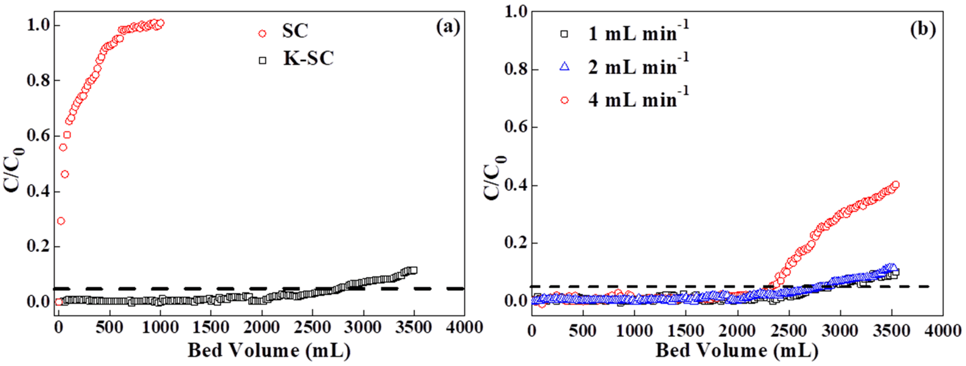

FIG. 8 (a) The elimination efficiency curves of TC retained by SC and K-SC; (b) Effects of flow rate on the elimination of TC. Experimental conditions: original TC contents=5.0 mg/L, adsorbents contents=0.1 g, initial pH=7.0, temperature=25 °C.

displayed in FIG. 8(b), the effective filtration volume remains unchanged with the increment of flow rate from 1.0 mL/min to 2.0 mL/min; whereas, it decreases from 2780 BV to 2320 BV with flow rate sequentially raising to 4.0 mL/min, indicating that the residence time of TC in the column is insufficient to reach the adsorption equilibrium at 4.0 mL/min, consequently causing a reduction in removal efficiency. To summarize, both batch sorption and continuous-flowing column experiments reveal that the fabricated K-SC is a promising amendments for TC elimination in real aqueous environment.

IV. CONCLUSION

In summary, K-SC featuring hierarchically porous structure and ultrahigh specific surface areas have been satisfactorily fabricated via a simple calcination of seaweeds and subsequently KOH activation for highly effective TC removal. Thanks to the integrated merits of high surface area, abundant functional groups and hierarchical pores, K-SC can rapidly remove high and low concentrations of TC, which is superior to other reported TC adsorbents. Meanwhile, the obtained K-SC exhibits preferable anti-interference capability towards TC, in which π-π interactions assume primary responsibility for the uptake of TC on K-SC. Furthermore, the fixed-bed column adsorption experiments demonstrate the fabricated K-SC possesses superior effective filtration volume. Hence, the present study will provide new perspectives on the fabrication of low-cost, extensively applicable and efficient adsorbents for *in-situ* TC elimination from environment.

Supplementary materials: The detailed experimental sections including materials, characterizations of SC and K-SC, batch adsorption experiments and fixed bed adsorption studies; Langmuir and Freundlich isotherm model; parameters of tetracycline; experimental apparatus for fixed bed column adsorption; XRD, Raman and FT-IR spectra of SC and K-SC; FT-IR and XPS spectra of pristine K-SC and after binding TC are available.

V. ACKNOWLEDGMENTS

This work was supported supported by the National Key R&D Program of China (2017YFA0207202) and the National Natural Science Foundation of China (No.41701259, No.51572263, and No.51772299).

[1] N. Wu, M. Qiao, B. Zhang, W. D. Cheng, and Y. G. Zhu, Environ. Sci. Technol. **44**, 6933 (2010).
[2] T. H. Le, C. Ng, N. H. Tran, H. Chen, and K. Y. H. Gin, Water Res. **145**, 498 (2018).
[3] F. Wang, S. Ma, Y. Si, L. F. Dong, X. L. Wang, J. Yao, H. L. Chen, Z. J. Yi, W. C. Yao, and B. S. Xing, Carbon **114**, 671 (2017).
[4] C. Gu and K. G. Karthikeyan, Environ. Sci. Technol. **39**, 2660 (2005).
[5] C. W. Knapp, J. Dolfing, P. A. Ehlert, and D. W. Graham, Environ. Sci. Technol. **44**, 580 (2010).
[6] Y. J. Wang, D. A. Jia, R. J. Sun, H. W. Zhu, and D. M. Zhou, Environ. Sci. Technol. **42**, 3254 (2008).
[7] J. Bai, Y. Liu, J. Li, B. Zhou, Q. Zheng, and W. Cai, Appl. Catal. B-Environ. **98**, 154 (2010).
[8] X. D. Zhu, Y. J. Wang, R. J. Sun, and D. M. Zhou, Chemosphere **92**, 925 (2013).
[9] J. Wang, X. G. Duan, Q. Dong, F. P. Meng, X. Y. Tan, S. M. Liu, and S. B. Wang, Carbon **144**, 781 (2019).
[10] Y. L. Zou, H. Huang, M. Chu, J. W. Lin, D. Q. Yin, and Y. N. Li, Adv. Mater. Res. **573**, 43 (2012).
[11] Y. Zhao, J. Geng, X. Wang, X. Gu, and S. Gao, J. Colloid Interf. Sci. **361**, 247 (2011).
[12] M. Ersan, U. A. Guler, U. Acıkel, and M. Sarioglu, Process Saf. Environ. Prot. **96**, 22 (2015).
[13] W. Xiong, G. Zeng, Z. Yang, Y. Zhou, C. Zhang, M. Cheng, Y. Liu, L. Hu, J. Wan, and C. Zhou, Sci. Total Environ. **627**, 235 (2018).

[14] B. Huang, Y. Liu, B. Li, S. Liu, G. Zeng, Z. Zeng, X. Wang, Q. Ning, B. Zheng, and C. Yang, Carbohydr. Polym. **157**, 576 (2017).

[15] Y. Lin, S. Xu, and J. Li, Chem. Eng. J. **225**, 679 (2013).

[16] X. Zhu, Y. Liu, C. Zhou, G. Luo, S. Zhang, and J. Chen, Carbon **77**, 627 (2014).

[17] R. Acosta, V. Fierro, A. Martinez de Yuso, D. Nabarlatz, and A. Celzard, Chemosphere **149**, 168 (2016).

[18] L. Ji, Y. Wan, S. Zheng, and D. Zhu, Environ. Sci. Technol. **45**, 5580 (2011).

[19] D. Zhang, J. Yin, J. Zhao, H. Zhu, and C. Wang, J. Environ. Chem. Eng. **3**, 1504 (2015).

[20] J. Han, J. H. Kwon, J. W. Lee, J. H. Lee, and K. C. Roh, Carbon **118**, 431 (2017).

[21] Y. Chen, F. Wang, L. Duan, H. Yang, and J. Gao, J. Mol. Liq. **222**, 487 (2016).

[22] S. Fan, Y. Wang, Y. Li, Z. Wang, Z. Xie, and J. Tang, Environ. Sci. Pollut. Res. **25**, 29529 (2018).

[23] A. C. Martins, O. Pezoti, A. L. Cazetta, K. C. Bedin, D. A. Yamazaki, G. F. Bandoch, T. Asefa, J. V. Visentainer, and V. C. Almeida, Chem. Eng. J. **260**, 291 (2015).

[24] W. Yang, F. Zheng, Y. Lu, X. Xue, and N. Li, Ind. Eng. Chem. Res. **50**, 13892 (2011).

[25] H. A. Khalil, C. K. Saurabh, Y. Tye, T. Lai, A. Easa, E. Rosamah, M. Fazita, M. Syakir, A. Adnan, and H. Fizree, Renew. Sust. Energy Rev. **77**, 353 (2017).

[26] D. A. Roberts, N. A. Paul, S. A. Dworjanyn, M. I. Bird, and R. De Nys, Sci. Rep. **5**, 9665 (2015).

[27] D. J. Malik, S. V. Jr, M. Streat, and A. M. Puziy, Water Res. **36**, 1527 (2002).

[28] W. Chen, H. Yang, Y. Chen, K. Li, M. Xia, and H. Chen, Environ. Sci. Technol. **52**, 9514 (2018).

[29] N. Sun, Z. Li, X. Zhang, W. Qin, C. Zhao, H. Zhang, D. H. Ng, S. Kang, H. Zhao, and G. Wang, ACS Sustainable Chem. Eng. **7**, 8735 (2019).

[30] S. B. Velasquez-Orta, T. P. Curtis, and B. E. Logan, Biotechnol. Bioeng. **103**, 1068 (2009).

[31] J. Wang and S. Kaskel, J. Mater. Chem. **22**, 23710 (2012).

[32] Y. Tian, B. Gao, V. L. Morales, H. Chen, Y. Wang, and H. Li, Chemosphere **90**, 2597 (2013).

[33] S. W. L. Ng, G. Yilmaz, W. L. Ong, and G. W. Ho, Appl. Catal. B-Environ. **220**, 533 (2018).

[34] S. Lee, D. Kwak, S. Han, Y. Lee, J. Lee, I. Choi, H. Park, J. Y. Park, and K. Park, ACS Catal. **6**, 5095 (2016).

[35] Q. Long, W. Chen, H. Xu, X. Xiong, Y. Jiang, F. Zou, X. Hu, Y. Xin, Z. Zhang, and Y. Huang, Energy Environ. Sci. **6**, 2497 (2013).

[36] T. Chen, L. Luo, S. Deng, G. Shi, S. Zhang, Y. Zhang, O. Deng, L. Wang, J. Zhang, and L. Wei, Bioresour. Technol. **267**, 431 (2018).

[37] O. Pezoti Jr, A. L. Cazetta, I. P. Souza, K. C. Bedin, A. C. Martins, T. L. Silva, and V. C. Almeida, J. Ind. Eng. Chem. **20**, 4401 (2014).

[38] Q. Zhou, Z. Li, C. Shuang, A. Li, M. Zhang, and M. Wang, Chem. Eng. J. **210**, 350 (2012).

[39] O. Pezoti, A. L. Cazetta, K. C. Bedin, L. S. Souza, A. C. Martins, T. L. Silva, O. O. S. Jnior, J. V. Visentainer, and V. C. Almeida, Chem. Eng. J. **288**, 778 (2016).

[40] H. M. Jang and E. Kan, Bioresour. Technol. **274**, 162 (2019).

[41] M. Ahmed, M. A. Islam, M. Asif, and B. Hameed, Bioresour. Technol. **243**, 778 (2017).

[42] M. H. Marzbali, M. Esmaieli, H. Abolghasemi, and M. H. Marzbali, Process Saf. Environ. Prot. **102**, 700 (2016).

[43] P. Liu, W. J. Liu, H. Jiang, J. J. Chen, W. W. Li, and H. Q. Yu, Bioresour. Technol. **121**, 235 (2012).

[44] X. Yang, G. Xu, H. Yu, and Z. Zhang, Bioresour. Technol. **211**, 566 (2016).

[45] T. Selmi, A. Sanchez-Sanchez, P. Gadonneix, J. Jagiello, M. Seffen, H. Sammouda, A. Celzard, and V. Fierro, Ind. Crop. Prod. **115**, 146 (2018).

[46] X. Zhu, Y. Liu, F. Qian, C. Zhou, S. Zhang, and J. Chen, Bioresour. Technol. **154**, 209 (2014).

[47] C. Peiris, S. R. Gunatilake, T. E. Mlsna, D. Mohan, and M. Vithanage, Bioresour. Technol. **246**, 150 (2017).

[48] X. R. Jing, Y. Y. Wang, W. J. Liu, Y. K. Wang, and H. Jiang, Chem. Eng. J. **248**, 168 (2014).

DOI:10.1063/1674-0068/cjcp2009154